

Zero-shot Generalizable Graph Anomaly Detection with Mixture of Riemannian Experts

Xinyu Zhao, Qingyun Sun, *Member, IEEE*, Jiayi Luo, Xingcheng Fu, Jianxin Li, *Senior Member, IEEE*

Abstract—Graph Anomaly Detection (GAD) aims to identify irregular patterns in graph data, and recent works have explored zero-shot generalist GAD to enable generalization to unseen graph datasets. However, existing zero-shot GAD methods largely ignore intrinsic geometric differences across diverse anomaly patterns, substantially limiting their cross-domain generalization. In this work, we reveal that anomaly detectability is highly dependent on the underlying geometric properties and that embedding graphs from different domains into a single static curvature space can distort the structural signatures of anomalies. To address the challenge that a single curvature space cannot capture geometry-dependent graph anomaly patterns, we propose **GAD-MoRE**, a novel framework for zero-shot Generalizable Graph Anomaly Detection with a Mixture of Riemannian Experts architecture. Specifically, to ensure that each anomaly pattern is modeled in the Riemannian space where it is most detectable, GAD-MoRE employs a set of specialized Riemannian expert networks, each operating in a distinct curvature space. To align raw node features with curvature-specific anomaly characteristics, we introduce an anomaly-aware multi-curvature feature alignment module that projects inputs into parallel Riemannian spaces, enabling the capture of diverse geometric characteristics. Finally, to facilitate better generalization beyond seen patterns, we design a memory-based dynamic router that adaptively assigns each input to the most compatible expert based on historical reconstruction performance on similar anomalies. Extensive experiments in the zero-shot setting demonstrate that GAD-MoRE significantly outperforms state-of-the-art generalist GAD baselines, and even surpasses strong competitors that are few-shot fine-tuned with labeled data from the target domain.

Index Terms—Graph Anomaly Detection, Mixture of Experts, Riemannian Graph Learning, Zero-shot Learning.

I. INTRODUCTION

GRAPH Anomaly Detection (GAD) [1], [2] aims to identify irregular patterns in graph-structured data. Detecting such anomaly patterns is of significant practical importance in many real-world applications [3], as they often correspond to detrimental events and abnormal behaviors, such as financial fraud rings characterized by dense clique formations [4], [5] or misinformation campaigns exhibiting star-like spreading patterns [6], [7], [8], which can ultimately lead to severe financial losses and negative social consequences. Benefiting from the powerful representation learning capability of Graph Neural Networks (GNNs), numerous GAD methods incorporate GNNs into their frameworks [9], [10]. However, the

X. Zhao, Q. Sun, J. Luo, and J. Li are with the School of Computer Science and Engineering, Beihang University, Beijing 100191, China (Email: {xyzhao, sunqy, luojy, lijx}@buaa.edu.cn).

X. Fu is with the Key Lab of Education Blockchain and Intelligent Technology, Ministry of Education, Guangxi Normal University, Guilin 541004, China (E-mail: fuxc@gxnu.edu.cn).

Manuscript received December 1, 2025.

majority of existing methods are designed under a restrictive assumption: training and inference are performed on the same graph. This paradigm inherently limits practical applicability, where the structural and attribute patterns that characterize anomalous behavior are not universal across graphs [2]. For example, the topology of a spam-bot community in a social network [6] can be entirely different from that of a financial fraud ring in a transaction graph [5]. As a result, models trained within a single domain tend to overfit to their specific anomaly patterns, failing to generalize to unseen graphs without costly retraining and labeling. This inability to transfer learned anomaly patterns across varying distributions constitutes a critical generalization challenge [2], [10].

To enable cross-graph generalization, recent works have begun to explore zero-shot or few-shot GAD models [16], [17], [18], [19]. While these approaches have made promising progress, *they often overlook the critical issue that different anomaly patterns exhibit substantial geometric heterogeneity across graphs*. As a result, their ability to generalize to new, unseen graph domains remains limited. Under this heterogeneity, representing all graphs in a single fixed-curvature space can introduce systematic embedding distortion, where certain structural relations are over-compressed or over-stretched, reducing separability and making subtle anomalies harder to distinguish from normal variability. Geometry acts as an inductive bias that shapes which structural properties are explicitly captured. For example, in hierarchical graphs, anomalous bridge nodes linking distant branches are naturally exposed as outliers in hyperbolic space with negative curvature [20]. By contrast, graphs with dense structures are better captured in spherical space, where anomalies typically manifest as isolated nodes deviating from clusters [13], [21]. Therefore, imposing a single fixed-curvature across all graphs ignores the geometric heterogeneity of anomaly patterns, potentially distorting anomaly representations. To examine the geometric heterogeneity of graph anomalies, we conduct a preliminary study on representative datasets, with the results shown in Figure 1. Specifically, we use a standard Graph Autoencoder (GAE) [22] to learn node embeddings in constant-curvature spaces with different curvature values, and then evaluate anomaly detection performance using classical unsupervised detectors, including K-Means [11], k-NN [12], and Isolation Forest [13]. As shown in Figure 1, performance varies substantially with the choice of curvature. For example, the Weibo [14] dataset shows a clear performance peak in Euclidean space ($\kappa = 0.0$), whereas the Citeseer and Cora [15] datasets consistently prefer positive curvature spaces, and the Amazon [7] dataset exhibits a preference for negative curvature. These results motivate that

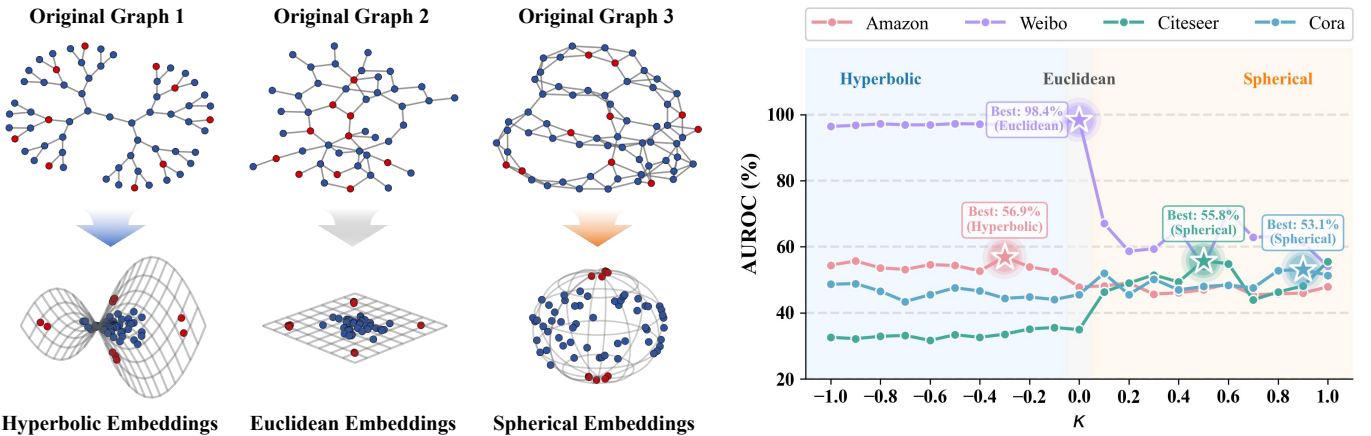


Fig. 1: The left part illustrates the projection of graph structures into Hyperbolic ($\kappa < 0$), Euclidean ($\kappa = 0$), and Spherical ($\kappa > 0$) spaces. It highlights that anomalous nodes (red), which are intrinsically hidden within the original graph topology, become significantly more separable and detectable from normal nodes (blue) once mapped into these Riemannian manifolds. The right part quantifies this effect by showing the average AUROC performance of representative GAD methods (including K-Means [11], k-NN [12], and Isolation Forest [13]) across varying curvature values $\kappa \in [-1.0, 1.0]$ on four datasets: Amazon [7], Weibo [14], Cora [15], and CiteSeer [15].

different anomalies are more effectively detected in different Riemannian spaces, making fixed-curvature embeddings sub-optimal for anomaly detection. Consequently, it is essential to develop an adaptive framework that can dynamically align the Riemannian representation with the anomaly patterns of each graph. To overcome the limitation that a single fixed Riemannian space cannot capture curvature-dependent anomaly patterns across different graphs, we propose GAD-MoRE, a novel framework for zero-shot generalizable Graph Anomaly Detection with a Mixture of Riemannian Experts architecture, explicitly designed to model geometric heterogeneity in graph anomaly patterns. Specifically, to ensure each anomaly pattern is modeled in the geometry where it is most detectable, we first employ a collection of specialized Riemannian expert networks within the MoE architecture. Unlike single-geometry models that distort structural patterns, each expert operates in a distinct curvature space, enabling distinct anomaly patterns to be captured in their suitable Riemannian space. Second, to transform raw node features into geometry-sensitive representations that are suitable for these Riemannian experts, we introduce an anomaly-aware multi-curvature feature alignment module. This component bridges the gap between geometry-agnostic attributes and Riemannian manifolds, producing robust representations compatible with diverse experts. Finally, to route each node to its most appropriate Riemannian expert, we design a memory-based dynamic router that adaptively assigns current input nodes according to each expert's historical anomaly detection performance, thereby enhancing generalization to unseen data. Extensive experiments demonstrate that our proposed GAD-MoRE achieves state-of-the-art zero-shot GAD performance, notably surpassing strong competitors even when they are fine-tuned with labeled target domain data.

Our contributions can be summarized as follows:

- We show that graph anomalies exhibit geometric heterogeneity, where different anomaly patterns have different

detectability in distinct Riemannian spaces, whereas a single fixed Riemannian space is inherently insufficient to capture them.

- We propose a novel zero-shot generalizable graph anomaly detection framework named GAD-MoRE, which explicitly models the graph anomaly geometric heterogeneity via a mixture of Riemannian experts coupled with an anomaly-aware multi-curvature feature alignment module and a memory-based dynamic router.
- Extensive experiments demonstrate that GAD-MoRE significantly outperforms state-of-the-art baselines in challenging zero-shot settings, even against competitors fine-tuned with target-domain labels.

Organization: The subsequent sections of this paper are structured as follows. We begin by surveying the relevant literature in Section II. Next, Section III provides the formal problem definition and essential background. The technical architecture of the proposed GAD-MoRE is detailed in Section IV, followed by a thorough performance evaluation in Section V. We provide concluding remarks and future outlooks in Section VI.

II. RELATED WORK

A. Graph Anomaly Detection

Our work focuses on node-level graph anomaly detection (GAD), which aims to identify anomalous nodes in graph-structured data [2]. Existing methods can be broadly categorized into supervised, unsupervised, and general methods.

(1) *Supervised Methods.* Supervised methods formulate GAD as a node classification problem using graph neural networks (GNNs). These approaches fall into two main categories: discriminative and generative GNNs [10]. Discriminative models such as CARE-GNN [23] and GHRN [24] improve neighborhood aggregation and feature transformation to separate normal and anomalous nodes, leveraging techniques

like edge selection [23] and edge synthesis [24]. Generative models such as GraphSMOTE [25], GraphMixup [26], and GODM [27] generate synthetic anomalies. They typically rely on feature interpolation [25], [26] or noise perturbation [27] to augment training data and mitigate label scarcity. *While these methods perform well when labeled data is available, they are constrained by the high cost of anomaly labels.*

(2) *Unsupervised Methods.* Unsupervised methods do not require labeled anomalies and instead rely on proxy tasks to guide model learning [10]. Common strategies include graph reconstruction, graph contrastive learning, graph knowledge distillation, adversarial training, and score prediction. Reconstruction-based models such as DOMINANT [28], AnomalyDAE [29], and GUIDE [30] reconstruct node features or graph structures, with reconstruction errors serving as anomaly scores. Contrastive learning methods such as DGI [31], InfoGraph [32], and CoLA [21] train models to separate similar and dissimilar samples to improve anomaly discrimination. Knowledge distillation models such as GLADST [33] transfer stable representations from teacher to student models. Adversarial methods like AEGIS [34] and GAAN [35] use generator-discriminator frameworks to simulate challenging examples and improve generalization. Score prediction models, including Meta-GDN [36] and SAD [37], directly learn node-level anomaly scores within a unified framework. These approaches perform well without supervision and have benefited from recent advances in deep learning, *but still face challenges in aligning proxy tasks with anomaly objectives and modeling the structural and attribute heterogeneity inherent across graphs.*

(3) *Generalizable Methods.* Most existing GAD methods are designed for specific graphs and depend heavily on task-specific training, making them difficult to transfer across graph domains. They often assume consistent structural patterns and anomaly types, limiting their effectiveness in real-world scenarios where graphs differ widely in topology, semantics, and context. Moreover, such models typically require retraining on each new graph, which is computationally expensive and often impractical. To address these limitations, generalizable GAD methods [16], [17], [18], [19] aim to support anomaly detection across diverse graph domains, enabling few-shot or zero-shot transfer. ARC [16] applies contextual learning to adapt models with limited target labels, but struggles in fully zero-shot scenarios. UNPrompt [17] introduces a unified neighborhood prompting mechanism to detect anomalies without labels, although its performance is highly sensitive to the source graph structure. More recently, AnomalyGFM [18] proposes a graph foundation architecture. This approach distinguishes between normal and anomalous categories by mapping node residual errors into a common embedding space to match domain-invariant prototypes. Parallelly, IA-GGAD [19] advances this frontier by learning invariant representations and structure-insensitive affinities, aiming to mitigate the impact of domain-specific structural noise. These approaches offer promising generalization capability but remain vulnerable to structural inconsistencies and distribution shifts across domains. *However, none of these approaches explicitly address the intrinsic geometric heterogeneity across graphs, which we*

TABLE I: Summary of Key Notations.

Symbol	Definition
<i>Graph Structure & Attributes</i>	
\mathcal{G}	An attributed graph.
\mathcal{V}	The set of nodes.
\mathcal{E}	The set of edges.
\mathbf{A}	Adjacency matrix, $\mathbf{A} \in \{0, 1\}^{N \times N}$.
N	The number of nodes.
D	The dimension of the unified node features.
\mathbf{X}_0	The raw node feature matrix with original dimensions.
\mathbf{X}	The unified node feature matrix, $\mathbf{X} \in \mathbb{R}^{N \times D}$.
<i>Anomaly Detection Task</i>	
\mathcal{V}_a	The set of anomalous nodes.
\mathcal{V}_n	The set of normal nodes.
\mathbf{y}	The ground-truth label vector, $\mathbf{y} \in \{0, 1\}^N$.
f	An anomaly scoring function, $f : \mathcal{V} \rightarrow \mathbb{R}$.
$\mathcal{D}_{\text{train}}$	The set of source graphs for training.
$\mathcal{D}_{\text{test}}$	The set of unseen target graphs for testing.
<i>Model Concepts</i>	
\mathcal{M}	A Riemannian manifold.
κ	The constant sectional curvature of a manifold.
$T_p \mathcal{M}$	The tangent space at point p on the manifold \mathcal{M} .
K	The number of experts in the MoE model.
E_i	The i -th expert network in the MoE model.
G	The gating network in the MoE model.
<i>Riemannian Geometry</i>	
$d_{\mathcal{E}}(p, q)$	The Euclidean distance between points p and q .
$d_{\mathcal{H}}(p, q)$	The hyperbolic distance between points p and q .
$d_{\mathcal{S}}(p, q)$	The spherical distance between points p and q .
\exp_p	The exponential map at point p on the manifold.
\log_p	The logarithmic map at point p on the manifold.

find is essential for generalizable GAD.

B. Mixture of Experts for Graph Learning

Mixture-of-Experts (MoE) architecture [38], [39] leverages a gating network to dynamically assign inputs to specialized expert models, thereby enabling conditional computation and scalable model capacity [40]. This design allows different experts to focus on distinct data characteristics while maintaining computational efficiency. While MoE has achieved notable success in large-scale language and vision models [41], [42], [43], its adoption in graph learning remains relatively limited, though recent efforts suggest a growing interest in this direction. Recent studies [44], [45], [46] in graph learning have explored MoE frameworks to address structural and distributional heterogeneity inherent in graph data. For example, GraphDIVE [47] and G-FAME [46] route minority or under-represented nodes to dedicated experts, aiming to improve performance under data imbalance and fairness constraints. Other works implicitly adopt the MoE philosophy by varying message-passing depths or spectral filters, effectively treating different configurations as expert modules to diversify receptive fields and capture multi-scale graph structures. Beyond structural routing, MoW [45] decouples feature and structure modalities to enable specialized processing, whereas GraphMoRE [44] introduces curvature-aware experts to adapt to geometric variation across graph representations. In the context of anomaly detection, MoEGAD [48] presents the first exploration of MoE architecture in Graph-Level Anomaly Detection, leveraging a latent MoE module and iterative

anomalous graph generation to overcome the scarcity of labeled anomalies. Despite these advances, existing MoE-based graph methods primarily focus on supervised tasks such as node classification within a single graph domain. In contrast, the potential of a geometry-aware MoE framework for the distinct and more challenging problem of domain-general graph anomaly detection remains largely unexplored. In this work, we investigate how expert specialization and gating mechanisms can be leveraged to bridge distribution shifts across domains and enable zero-shot GAD without requiring exhaustive retraining.

C. Riemannian Graph Learning

Many real-world graphs exhibit hierarchical or tree-like organizations, which are inherently difficult to model in Euclidean space [49]. As a result, Riemannian graph learning [50], [51] has emerged as a powerful and principled paradigm that embeds graph data into curved manifolds, most notably hyperbolic spaces, to capture these intrinsic geometric properties with significantly lower distortion [52], [53], [43]. By generalizing GNN operations, such as message passing and aggregation, to these curved spaces, hyperbolic GNNs [54], [55] are able to more faithfully encode structural priors and relational patterns present in complex graphs. While these geometric methods have proven effective, their application has predominantly focused on supervised learning within a single graph domain. The potential of leveraging diverse geometric priors from multiple curvature spaces for domain-general anomaly detection remains largely unexplored. In this work, we propose a mixture of Riemannian experts architecture for generalizable GAD, where each expert operates in a distinct Riemannian manifold, enabling the model to effectively identify anomalies across graphs.

III. PRELIMINARIES

This section formally defines the core problem and notations in this paper, and briefly reviews the necessary background on curvature manifolds.

A. Notations and Problem Formulation

Key Notations: Our research focuses on the task of anomaly detection at the node level. To facilitate a clear understanding of the framework, Table I organizes the essential symbols employed throughout this study. Formally, we represent an attributed graph as $\mathcal{G} = (\mathcal{V}, \mathcal{E}, \mathbf{X})$, where the components \mathcal{V} , \mathcal{E} , and \mathbf{A} correspond to the node set, the set of edges, and the adjacency matrix, respectively. The node set \mathcal{V} is partitioned into anomalous nodes \mathcal{V}_a and normal nodes \mathcal{V}_n , where $|\mathcal{V}_a| \ll |\mathcal{V}_n|$. The goal of Graph Anomaly Detection (GAD) is to learn a scoring function $f : \mathcal{V} \rightarrow \mathbb{R}$ such that $f(v_a) > f(v_n)$ for $v_a \in \mathcal{V}_a, v_n \in \mathcal{V}_n$.

Problem Formulation: Our work focuses on the generalizable GAD paradigm. A model is trained on a set of source graphs $\mathcal{D}_{\text{train}} = \{\mathcal{G}^{(1)}, \dots, \mathcal{G}^{(M)}\}$ and evaluated on a set of unseen target graphs $\mathcal{D}_{\text{test}} = \{\mathcal{G}^{(M+1)}, \dots, \mathcal{G}^{(P)}\}$, where $\mathcal{D}_{\text{train}} \cap \mathcal{D}_{\text{test}} = \emptyset$. We address the zero-shot setting, where no

labeled data or fine-tuning on the target graphs is permitted. To ensure a unified model input, raw feature matrices $\mathbf{X}_0^{(i)}$ with varying dimensionalities across different datasets are projected into a shared D -dimensional feature space $\mathbf{X} \in \mathbb{R}^{N \times D}$.

B. Constant Curvature Manifolds

Our method leverages Riemannian manifolds with constant curvature (κ) to model diverse graph structures. Specifically, we consider three types of manifolds, as described below:

- **Euclidean Space** ($\kappa = 0$): A flat Riemannian space equipped with the ℓ_2 -norm distance, defined as:

$$d_E(p, q) = \|p - q\|_2. \quad (1)$$

- **Hyperbolic Space** ($\kappa < 0$): A negatively curved hyperbolic space is well suited for modeling hierarchical and tree-like structures. Under the Poincaré ball model, the distance between two points is defined as:

$$d_H(p, q) = \frac{1}{\sqrt{-\kappa}} \operatorname{arccosh} \left(1 + \frac{2\|p - q\|^2}{(1 + \kappa\|p\|^2)(1 + \kappa\|q\|^2)} \right). \quad (2)$$

- **Spherical Space** ($\kappa > 0$): A positively curved spherical space that is well-suited for modeling cyclical or periodic structures. The distance is defined as:

$$d_S(p, q) = \frac{1}{\sqrt{\kappa}} \arccos(\langle p, q \rangle). \quad (3)$$

The choice of curvature κ fundamentally influences the geometric properties of the embedding space and its suitability for modeling different graph structures.

IV. THE PROPOSED GAD-MORE FRAMEWORK

Graph Anomaly Detection (GAD) faces a critical generalization challenge: models trained on specific graphs struggle to transfer learned anomaly patterns to unseen graphs due to substantial shifts in topology and anomaly characteristics. As demonstrated in Section I, graph anomaly patterns exhibit geometric heterogeneity, *i.e.*, variability in underlying curvature across graph domains. Enforcing diverse graph structures into a single fixed-curvature space inevitably distorts the distinct structural patterns that define anomalies, hindering discrimination between normal and anomalous nodes. Geometry acts as a critical inductive bias: performance is highly sensitive to the chosen Riemannian space, with different datasets exhibiting distinct curvature preferences, and no single geometry proves universally optimal.

To overcome the limitations of single-curvature representation, we propose GAD-MoRE, a novel Geometric-aware framework for zero-shot Generalizable Graph Anomaly Detection with a Mixture-of-Experts architecture that integrates three coordinated components to effectively resolve the conflicts arising from geometric heterogeneity. The overall architecture is illustrated in Figure 2, which is coupled with three critic modules:

- **Anomaly-aware Multi-curvature Feature Alignment:** As the foundational step, this module projects and aligns raw node features from various sources and dimensions into a unified geometry-aware feature space. By processing features in

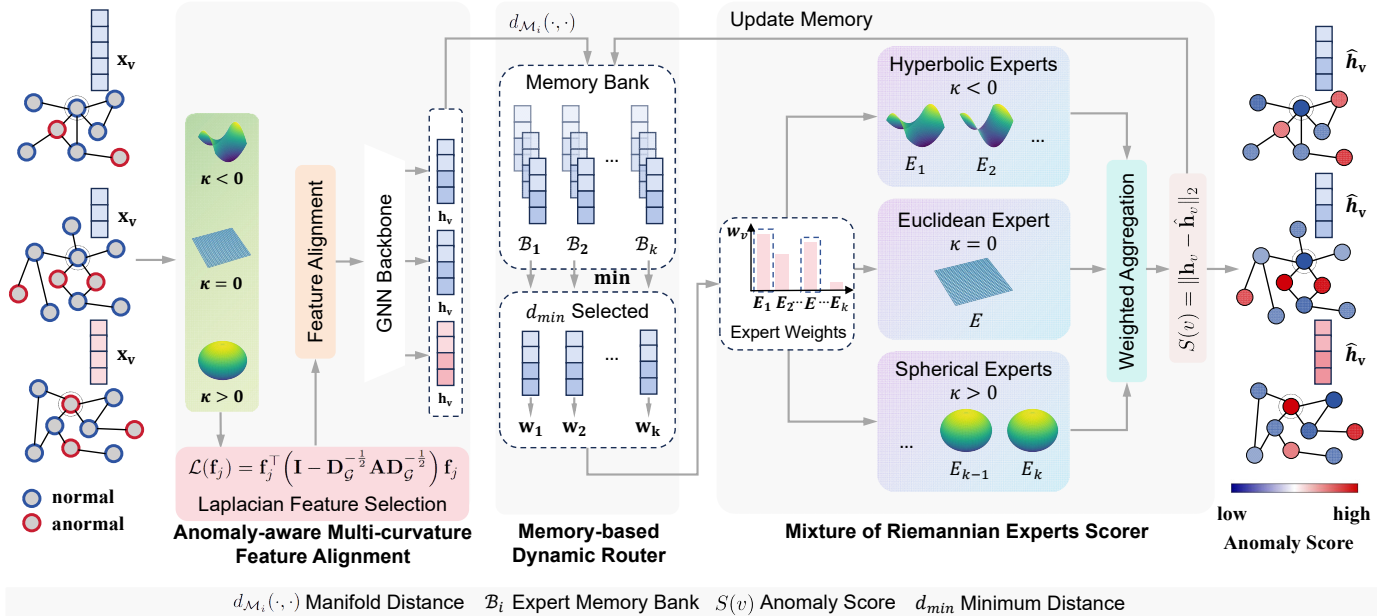


Fig. 2: The overall architecture of the GAD-MoRE framework. (1) The Anomaly-aware Multi-curvature Feature Alignment module projects raw features into a unified, geometry-aware representation. (2) The Mixture of Riemannian Experts Scorer utilizes a GNN backbone to encode structural context and employs specialized Riemannian expert networks. (3) The Memory-based Dynamic Router adaptively assigns nodes to these experts based on historical reconstruction quality to compute the final anomaly score.

parallel across multiple curvature manifolds, it produces representations enriched with diverse geometric information.

- **Memory-based Dynamic Router:** This module assigns each node to the most suitable Riemannian expert based on current structural features together with previously learned patterns, thereby improving expert assignment on unseen data and enhancing overall generalization.
- **Mixture of Riemannian Experts Scorer:** This module utilizes a lightweight graph encoder to capture structural context and employs a collection of specialized Riemannian expert networks. Each expert operates in a unique curvature space, enabling the model to capture disparate anomaly patterns without geometric distortion.

Together, these modules enable GAD-MoRE to dynamically adapt its geometric lens to the specific anomaly characteristics of each node, enabling effective zero-shot generalizable graph anomaly detection across diverse domains.

A. Anomaly-aware Multi-curvature Feature Alignment

Raw node features extracted from real-world graphs are inherently geometry-agnostic, as they exist in a flat Euclidean space without explicit geometric information. Yet, to effectively capture diverse structural patterns without distortion, our Riemannian expert networks must operate in distinct constant-curvature spaces.

This creates a fundamental mismatch: the Riemannian experts in MoE require manifold-aware inputs, while raw features lack geometric semantics. Simply feeding Euclidean features directly to curved-space experts is geometrically inconsistent and fails to leverage the representational advantages

of non-Euclidean geometries. Moreover, different graph domains exhibit preferences for different geometric curvatures, as demonstrated empirically in Section I.

To construct robust and generalizable inputs for Riemannian experts, we explicitly embed signals from multiple Riemannian spaces into the initial node features, preserving both the rich attribute information and global structural consistency.

To address this challenge, we introduce a feature alignment module that explicitly projects raw features into diverse Riemannian spaces before feeding them to the experts. Given a raw feature matrix \mathbf{X}_0 , the module performs a parallel transformation into a set of diverse Riemannian spaces, $\{\mathcal{M}_{\kappa_c}\}_{c=1}^C$. This set includes Euclidean space ($\kappa = 0$) alongside multiple curved spaces characterized by different constant negative ($\kappa < 0$) and positive curvatures ($\kappa > 0$). The total target feature dimension D is partitioned across these C spaces, such that $D = \sum_{c=1}^C D_c$, where D_c is the final dimensionality assigned to the c -th space. For curved spaces, the raw features are first mapped into the tangent space at the origin before further processing. To ensure that the features selected for each Riemannian space are both informative and dimensionally consistent, we employ a two-stage selection process:

Stage 1: Dimensionality Reduction. To construct geometry-specific feature candidates for each target manifold \mathcal{M}_c , we first project the raw features \mathbf{X}_0 into C parallel constant-curvature manifolds $\{\mathcal{M}_{\kappa_c}\}_{c=1}^C$. Specifically, for curved spaces, the raw attributes are mapped into the tangent space at the origin $T_{o_c} \mathcal{M}_c$ via the logarithmic map, thereby transforming geometry-agnostic features into manifold-aware representations. Then, we perform Principal Component Analysis (PCA) [56], [57] on these tangent-space features to extract

the principal components corresponding to each specific c -th curvature space. This step identifies the principal components of the feature space, capturing global high-variance attribute signals that are most informative for node discrimination.

Stage 2: Laplacian Feature Selection. We then compute the Laplacian score for each feature \mathbf{f}_j in the intermediate set \mathbf{X}'_c :

$$\mathcal{L}(\mathbf{f}_j) = \mathbf{f}_j^\top \left(\mathbf{I} - \mathbf{D}_G^{-\frac{1}{2}} \mathbf{A} \mathbf{D}_G^{-\frac{1}{2}} \right) \mathbf{f}_j, \quad (4)$$

where $\mathbf{D}_G = \text{diag}(\mathbf{A}\mathbf{1})$. Note that we omit the denominator term $\mathbf{f}_j^\top \mathbf{D}_G \mathbf{f}_j$ commonly used in the classical definition, consistent with our implementation. We then select the top- D_c features with the lowest scores to form the final feature set for that space, $\mathbf{X}_c^{\text{final}} \in \mathbb{R}^{N \times D_c}$. This selection ensures that the chosen features are smooth and consistent with the local graph topology, thus preserving crucial structural information essential for anomaly detection.

Ideally, PCA extracts high-variance attribute signals, while the subsequent Laplacian Score selection enforces structural consistency, yielding features that are both informative and geometrically meaningful. Finally, the selected features from all Riemannian spaces are concatenated to form a unified geometry-aware feature matrix $\mathbf{X} = \text{CONCAT}(\mathbf{X}_1^{\text{final}}, \dots, \mathbf{X}_C^{\text{final}}) \in \mathbb{R}^{N \times D}$.

The multi-curvature feature alignment module bridges the gap between geometry-agnostic raw features and the geometry-aware inputs required by the Riemannian expert networks. The resulting unified feature representation explicitly encodes signals from multiple curvature spaces while preserving both attribute richness and structural coherence, providing a robust foundation for the subsequent Riemannian experts to capture diverse graph anomaly patterns.

B. Mixture of Riemannian Experts Scorer

Different graph domains exhibit fundamentally different structural characteristics that are best captured in distinct Riemannian spaces. For instance, hierarchical graphs with tree-like structures are naturally suited for hyperbolic geometry, while graphs with dense, cyclical communities align better with positively curved spherical spaces. When anomalies are defined as deviations from these underlying structural patterns, enforcing all graphs into a single fixed-curvature space induces critical distortions. In a hyperbolic space, dense communities may explode and distort, making anomalous isolated nodes indistinguishable from the distorted normal nodes. Conversely, in a spherical space, hierarchical structures may be compressed, obscuring bridge nodes that improperly connect distant branches. This geometric mismatch makes it extremely difficult to distinguish subtle structural anomalies from normal variations. Effectively capturing diverse structural patterns without distortion requires an adaptive mechanism that represents nodes in their most suitable Riemannian space. This necessitates a unified architecture capable of accommodating multiple, potentially conflicting Riemannian representations. In the zero-shot setting, anomaly patterns across graph domains prefer different Riemannian representations, so a single learned curvature becomes a compromise, whereas a MoE formulation enables adaptive geometric selection.

Algorithm 1 The overall training pipeline of GAD-MoRE.

Require: Source graphs $\mathcal{D}_{\text{train}}$, number of experts K , active experts k , GNN hops L , loss weights $\{\lambda_j\}_{j=1}^5$, cold-start epochs E_{cold} .

Ensure: Trained model parameters Θ and expert memories $\{\mathcal{B}_j\}_{j=1}^K$.

```

1: /* Offline Preprocessing */
2: for  $i = 1, \dots, M$  do
3:   Align features:  $\mathbf{X}^{(i)} \leftarrow \text{MCFA}(\mathbf{X}_0^{(i)}, \mathbf{A}^{(i)})$ .
4:   Propagate structure:  $\{\mathbf{H}^{(l)}\}_{l=0}^L \leftarrow \text{Prop}(\mathbf{X}^{(i)}, \mathbf{A}^{(i)}, L)$ .
5: end for
6: /* Model Training */
7: Initialize expert memories  $\mathcal{B}_j \leftarrow \emptyset$  for  $j = 1, \dots, K$ .
8: for epoch = 1, ...,  $E_{\text{total}}$  do
9:   for each  $\mathcal{G}^{(i)} \in \mathcal{D}_{\text{train}}$  do
10:    /* Forward Pass */
11:    Encode structural context:  $\mathbf{H}_{\text{res}} \leftarrow \text{GNN}(\{\mathbf{H}^{(l)}\}_{l=0}^L)$ .
12:    Compute raw logits  $\mathbf{s}$  for all  $v \in \mathcal{V}$  by Eq. (8).
13:    Apply training noise:  $\tilde{\mathbf{s}} \leftarrow \mathbf{s} + \text{Noise}(\cdot)$ .
14:    Select top-k experts  $\mathcal{S}(v)$  and weights  $\mathbf{w}_v$  by Eq. (6).

15:    Reconstruct embeddings  $\hat{\mathbf{H}}$  by Eq. (7).
16:    Decode outputs:  $\hat{\mathbf{X}} \leftarrow \text{Dec}(\hat{\mathbf{H}})$ ,  $\hat{\mathbf{A}} \leftarrow \sigma(\hat{\mathbf{H}}\hat{\mathbf{H}}^\top)$ .
17:    /* Compute Losses */
18:    Compute reconstruction losses  $\mathcal{L}_{\text{embed}}, \mathcal{L}_{\text{feat}}, \mathcal{L}_{\text{struct}}$ .
19:    Compute  $\mathcal{L}_{\text{con}}$  by Eq. (17).
20:    Compute  $\mathcal{L}_{\text{gate}}$  by Eq. (18).
21:     $\mathcal{L}_{\text{total}} \leftarrow \sum_{j=1}^5 \lambda_j \mathcal{L}_j$  by Eq. (19).
22:    /* Optimization */
23:    Update parameters:  $\Theta \leftarrow \Theta - \eta \nabla_{\Theta} \mathcal{L}_{\text{total}}$ .
24:    /* Dynamic Memory Update */
25:    if epoch >  $E_{\text{cold}}$  then
26:      for  $j = 1, \dots, K$  do
27:        Compute quality scores  $q(v, j)$  by Eq. (11).
28:        Add high-quality samples to  $\mathcal{B}_j$  by Eq. (12).
29:      end for
30:    end if
31:  end for
32: end for

```

Node embeddings, which encode both multi-curvature attributes and structural context from the GNN backbone, are fed into the central innovation of GAD-MoRE: the mixture of Riemannian experts scorer. The GNN backbone first produces multi-hop feature matrices $\{\mathbf{H}^{(0)}, \dots, \mathbf{H}^{(K_{\text{hops}})}\}$ where $\mathbf{H}^{(0)} = \mathbf{X}$. A shared MLP Φ transforms $\{\mathbf{H}^{(0)}, \dots, \mathbf{H}^{(K_{\text{hops}})}\}$ into $\{\mathbf{X}'_k = \Phi(\mathbf{H}^{(k)})\}$. The final node embedding \mathbf{h}_v is then constructed using a residual formulation to capture structural deviations, defined as $\mathbf{h}_v = \text{CONCAT}(\mathbf{X}'_1(v) - \mathbf{X}'_0(v), \dots, \mathbf{X}'_{K_{\text{hops}}}(v) - \mathbf{X}'_0(v))$. This residual formulation is designed to explicitly capture how a node's representation evolves as structural information is aggregated from progressively larger neighborhoods. Large deviations between a node's initial features (\mathbf{X}'_0) and its aggregated features (\mathbf{X}'_k) indicate structural irregularity, providing a strong signal for

anomaly detection. This embedding \mathbf{h}_v is then input into the MoE scorer.

To simultaneously accommodate multiple Riemannian representations, we employ a Mixture-of-Experts (MoE) architecture with specialized Riemannian Expert Networks. The MoE model consists of a set of K expert networks, $\{E_i\}_{i=1}^K$. Each expert is a Riemannian expert, a small neural network designed to operate within a specific Riemannian manifold \mathcal{M}_{κ_i} with learnable curvature κ_i . Each expert E_i takes a node embedding \mathbf{h}_v from the Euclidean tangent space and computes its reconstruction $\hat{\mathbf{h}}_v^{(i)}$. This process involves mapping the input onto the manifold, processing it through manifold-aware layers, and mapping the result back to the tangent space:

$$\hat{\mathbf{h}}_v^{(i)} = \log_{o_i} (E_i (\exp_{o_i} (\mathbf{h}_v))), \quad (5)$$

where \exp_{o_i} and \log_{o_i} are the exponential and logarithmic maps at the origin o_i of the manifold \mathcal{M}_{κ_i} . This design allows different experts to specialize in reconstructing nodes that conform to different geometric priors, effectively capturing the diverse structural patterns present across graph domains. Following the practice of modern MoE, we employ sparse top- k routing to enable efficient conditional computation. For each node, the router first computes the gating weights $\mathbf{g}(\mathbf{h}_v)$ from the raw logits $\mathbf{s}(\mathbf{h}_v)$:

$$\mathbf{g}(\mathbf{h}_v) = \text{Softmax} \left(\frac{\mathbf{s}(\mathbf{h}_v)}{\tau} \right), \quad (6)$$

where the temperature is controlled by the parameter τ . From the computed probabilities, the top- k experts with maximal influence are selected for the active set $\mathcal{S}(v)$. The final output $\hat{\mathbf{h}}_v$ is computed as a weighted linear combination of outputs from these chosen experts, re-normalized among the k candidates:

$$\hat{\mathbf{h}}_v = \sum_{i \in \mathcal{S}(v)} \frac{\exp(s_i(\mathbf{h}_v)/\tau)}{\sum_{j \in \mathcal{S}(v)} \exp(s_j(\mathbf{h}_v)/\tau)} \cdot \hat{\mathbf{h}}_v^{(i)}. \quad (7)$$

This mechanism allows for expanded model capacity while keeping the per-node resource consumption manageable. As a result, GAD-MoRE is well-suited for large-scale applications, offering a scalable solution that still captures intricate geometric patterns effectively.

By deploying experts in distinct curvature spaces and adaptively selecting among them, GAD-MoRE represents nodes in their optimal geometric configuration, avoiding distortions inherent to fixed-geometry approaches and enabling accurate and generalizable detection of structural anomalies across diverse graph domains.

C. Memory-based Dynamic Router

With specialized Riemannian Expert Networks, each tailored to distinct structural patterns under its optimal curvature, the central routing challenge is to assign each node to the most suitable Riemannian expert for accurate anomaly scoring. Conventional routing mechanisms in MoE models typically rely on learned gating networks that predict expert assignments based on input features alone. For anomaly detection, however, the routing policy must be tightly coupled to the reconstruction

Algorithm 2 Inference Procedure of GAD-MoRE

Require: Test graph $\mathcal{G}_{\text{test}}(\mathbf{X}_0^{\text{test}}, \mathbf{A}^{\text{test}})$, trained model Θ , expert memories $\{\mathcal{B}_j\}_{j=1}^K$.
Ensure: Anomaly scores $S \in \mathbb{R}^{N_{\text{test}}}$.

```

1: /* Preprocessing */
2: Align features:  $\mathbf{X}^{\text{test}} \leftarrow \text{MCFA}(\mathbf{X}_0^{\text{test}}, \mathbf{A}^{\text{test}})$  by Eq. (4).
3: Propagate structure:  $\{\mathbf{H}^{(l)}\}_{l=0}^L \leftarrow \text{Prop}(\mathbf{X}^{\text{test}}, \mathbf{A}^{\text{test}}, L)$ .
4: /* Encoding & Routing */
5: Encode structural context:  $\mathbf{H}_{\text{res}} \leftarrow \text{GNN}(\{\mathbf{H}^{(l)}\}_{l=0}^L)$ .
6: for each node  $v \in \mathcal{V}_{\text{test}}$  do
7:   Compute logits  $\mathbf{s}_v: s_{v,j} \leftarrow -\min_{\mathbf{m} \in \mathcal{B}_j} d_{\mathcal{M}_j}(\dots)$  by Eq. (8).
8:   Calculate gating weights  $\mathbf{g}_v$  and select top- $k$  set  $\mathcal{S}(v)$  by Eq. (6).
9: end for
10: /* Reconstruction */
11: Reconstruct embeddings:  $\hat{\mathbf{H}} \leftarrow \sum_v \sum_{j \in \mathcal{S}(v)} w_{v,j} \cdot E_j(\mathbf{h}_{v,\text{res}})$  by Eq. (7).
12: /* Anomaly Scoring */
13: for each node  $v \in \mathcal{V}_{\text{test}}$  do
14:   Calculate score:  $S(v) \leftarrow \|\mathbf{h}_v - \hat{\mathbf{h}}_v\|_2$  by Eq. (20).
15: end for
16: return  $S$ .

```

objective: nodes should be directed to experts who can reconstruct their patterns with high fidelity, as reconstruction error directly determines the anomaly score. Without this alignment, the router may assign nodes to geometrically inappropriate experts, leading to unreliable anomaly scores and degraded detection performance. Moreover, a node's optimal Riemannian space depends on its historical reconstruction quality across different experts, which is not captured by feature-based routing alone. This motivates a routing mechanism capable of adaptively selecting experts based on their demonstrated ability to reconstruct similar patterns, thereby ensuring that the routing policy directly aligns with the anomaly detection objective.

To enable reconstruction quality-based routing, we propose a memory-based dynamic router that makes routing decisions based on historical performance patterns. Each expert E_i is equipped with an expert memory bank \mathcal{B}_i , which stores a collection of node embeddings $\{\mathbf{m}_{i,1}, \mathbf{m}_{i,2}, \dots\}$ that the expert has previously reconstructed with high fidelity. These memory banks serve as geometric prototypes, representing the patterns that each expert specializes in handling. For a given node embedding \mathbf{h}_v , the router computes its similarity to each memory bank. The raw routing logit $s_i(\mathbf{h}_v)$ for expert i is defined as the negative squared minimum manifold distance from \mathbf{h}_v to any embedding in the memory bank \mathcal{B}_i :

$$s_i(\mathbf{h}_v) = -\min_{\mathbf{m} \in \mathcal{B}_i} d_{\mathcal{M}_i}(\exp_{o_i}(\mathbf{h}_v), \exp_{o_i}(\mathbf{m})), \quad (8)$$

where $d_{\mathcal{M}_i}(\cdot, \cdot)$ is the distance metric on the manifold of expert i . This score measures how close node v is to the patterns that expert i is specialized in handling based on its historical reconstruction performance.

Expert Memory Banks are not static but are populated and refined dynamically throughout the training process to store a representative set of node embeddings that each expert reconstructs with high fidelity. The update mechanism is governed by a multi-stage strategy involving a cold-start period, a

dynamic quality gate, and a strategic replacement policy. The update process is triggered after each training batch. To allow the expert networks to stabilize before populating memory banks, we implement a cold-start period during which memory banks remain inactive. This prevents the storage of low-quality reconstructions from poorly initialized experts. After the cold-start period, for each expert E_i , we calculate a quality score $q(v, i)$ for each candidate node embedding \mathbf{h}_v assigned to it. Let $\mathcal{L}_{\text{recon}}(v, i) = \|\mathbf{h}_v - \hat{\mathbf{h}}_v^{(i)}\|_2^2$ be the reconstruction error, where $\hat{\mathbf{h}}_v^{(i)}$ is the reconstruction by expert E_i . We define the minimum and maximum errors within the current batch $\mathcal{B}_{\text{batch}}$ as:

$$\mathcal{L}_{\min}^{(i)} = \min_{v' \in \mathcal{B}_{\text{batch}}} \mathcal{L}_{\text{recon}}(v', i), \quad (9)$$

$$\mathcal{L}_{\max}^{(i)} = \max_{v'' \in \mathcal{B}_{\text{batch}}} \mathcal{L}_{\text{recon}}(v'', i). \quad (10)$$

The normalized quality score is:

$$q(v, i) = 1 - \frac{\mathcal{L}_{\text{recon}}(v, i) - \mathcal{L}_{\min}^{(i)}}{\mathcal{L}_{\max}^{(i)} - \mathcal{L}_{\min}^{(i)} + \epsilon}. \quad (11)$$

A dynamic quality gate is then applied to filter these candidates and select a high-quality subset \mathcal{C}_i^* exceeding a progressively stricter threshold $\tau_q(e)$ defined as a function of the current training epoch e :

$$\mathcal{C}_i^* = \{\mathbf{h}_v \mid q(v, i) \geq \tau_q(e)\}. \quad (12)$$

The threshold $\tau_q(e)$ increases linearly as training progresses, ensuring that the memory banks are populated with examples of progressively higher quality:

$$\tau_q(e) = \tau_{\min} + (\tau_{\max} - \tau_{\min}) \cdot \min \left(1, \frac{e - E_{\text{cold}}}{E_{\text{total}} - E_{\text{cold}}} \right), \quad (13)$$

where τ_{\min} and τ_{\max} are the start and end thresholds, and E_{cold} and E_{total} are the number of cold-start and total training epochs, respectively. To handle batches with universally low quality, the gate adaptively falls back to a percentile-based threshold. Once high-quality candidates in \mathcal{C}_i^* are selected, they are added to the memory bank \mathcal{B}_i . If a bank is full, a hysteretic replacement policy is enacted: a new candidate will only replace the existing embedding with the lowest quality score if its own quality surpasses it by a significant margin. This prevents noisy fluctuations and ensures memory stability. To avoid domination by any single batch, the number of embeddings added per update is also capped.

By adaptively assigning nodes based on historical reconstruction quality rather than feature similarity alone, the routing policy aligns expert selection with the anomaly detection objective, directing each node to the Riemannian space where it is best modeled.

From a modeling perspective, the proposed memory-based dynamic router provides a principled way to select experts based on reconstruction behavior, rather than relying on feature-based gating alone. Each Riemannian expert can be viewed as capturing a specific notion of normality under a given curvature prior, while its memory bank summarizes the regions of the embedding space where this expert has consistently achieved low reconstruction error. By routing

nodes according to historical reconstruction fidelity, the router effectively favors experts who are better suited to model similar structural patterns. This design naturally aligns the routing strategy with the anomaly detection objective, in which reconstruction error serves as the primary signal for identifying abnormal nodes.

D. Model Training and Optimization

GAD-MoRE is trained end-to-end in an unsupervised manner, as detailed in Algorithm 1. The total loss function $\mathcal{L}_{\text{total}}$ is a weighted sum of multiple components:

- *Embedding Reconstruction Loss ($\mathcal{L}_{\text{embed}}$)*: The primary reconstruction objective, defined as the Mean Squared Error:

$$\mathcal{L}_{\text{embed}} = \frac{1}{|\mathcal{V}|} \sum_{v \in \mathcal{V}} \|\mathbf{h}_v - \hat{\mathbf{h}}_v\|_2^2. \quad (14)$$

- *Feature Reconstruction Loss ($\mathcal{L}_{\text{feat}}$)*: This loss enforces the reconstructed embedding to preserve attribute information. A linear decoder maps the reconstructed embedding $\hat{\mathbf{h}}_v$ back to the original feature space, and the Mean Squared Error is computed against the original features \mathbf{X}_v :

$$\mathcal{L}_{\text{feat}} = \frac{1}{|\mathcal{V}|} \sum_{v \in \mathcal{V}} \|\mathbf{X}_v - \text{Decoder}_{\text{feat}}(\hat{\mathbf{h}}_v)\|_2^2. \quad (15)$$

- *Structure Reconstruction Loss ($\mathcal{L}_{\text{struct}}$)*: This loss preserves topological information. The adjacency matrix is reconstructed via an inner product of the reconstructed embeddings. Let $\hat{\mathbf{H}}$ be the matrix formed by stacking all reconstructed node embeddings $\hat{\mathbf{h}}_v$. The Binary Cross-Entropy (BCE) loss is then computed against the original adjacency matrix \mathbf{A} :

$$\mathcal{L}_{\text{struct}} = \text{BCE} \left(\sigma \left(\hat{\mathbf{H}} \hat{\mathbf{H}}^T \right), \mathbf{A} \right). \quad (16)$$

- *Structure-Contrastive Loss (\mathcal{L}_{con})*: This structure-aware InfoNCE loss encourages connected nodes to have similar representations. For a node v , the loss is:

$$\mathcal{L}_{\text{con}}(v) = -\log \frac{\sum_{u \in \mathcal{P}_v} \exp(\text{sim}(\mathbf{h}_v, \mathbf{h}_u) / \tau_c)}{\sum_{j \in \mathcal{V}} \exp(\text{sim}(\mathbf{h}_v, \mathbf{h}_j) / \tau_c)}, \quad (17)$$

where $\mathcal{P}_v = \{u \mid \mathbf{A}_{vu} = 1\}$ is the set of positive neighbors of v , and τ_c is a temperature parameter. For large graphs, the denominator is computed over a randomly sampled subset of nodes, consistent with our implementation.

- *Gate Entropy Regularization ($\mathcal{L}_{\text{gate}}$)*: This entropy-based loss encourages balanced router assignments and prevents expert collapse. To maximize entropy, we minimize its negative, which we define as the gate loss term:

$$\begin{aligned} \mathcal{L}_{\text{gate}} &= -\frac{1}{|\mathcal{V}|} \sum_{v \in \mathcal{V}} H(\mathbf{g}(\mathbf{h}_v)) \\ &= \frac{1}{|\mathcal{V}|} \sum_{v \in \mathcal{V}} \sum_{i=1}^K g_i(\mathbf{g}(\mathbf{h}_v)) \log g_i(\mathbf{g}(\mathbf{h}_v)). \end{aligned} \quad (18)$$

TABLE II: Statistics of the benchmark datasets.

Dataset	#Nodes	#Edges	#Feat.	#Anom. (%)
<i>Training Datasets</i>				
PubMed	19,717	44,338	500	600 (3.04)
Flickr	7,575	239,738	12,047	450 (5.94)
Reddit	10,984	168,016	64	366 (3.33)
YelpChi	23,831	49,315	32	1,217 (5.10)
<i>Test Datasets</i>				
ACM	16,484	71,980	8,337	597 (3.62)
Amazon	10,244	175,608	25	693 (6.76)
BlogCatalog	5,196	171,743	8,189	300 (5.77)
Citeseer	3,327	4,732	3,703	150 (4.50)
Cora	2,708	5,429	1,433	150 (5.53)
Facebook	1,081	55,104	576	25 (2.31)
Weibo	8,405	407,963	400	868 (10.30)

By integrating these modules with specific hyperparameters, the total training loss is established as follows:

$$\mathcal{L}_{\text{total}} = \lambda_1 \mathcal{L}_{\text{embed}} + \lambda_2 \mathcal{L}_{\text{feat}} + \lambda_3 \mathcal{L}_{\text{struct}} + \lambda_4 \mathcal{L}_{\text{con}} + \lambda_5 \mathcal{L}_{\text{gate}}, \quad (19)$$

where $\lambda_1, \lambda_2, \lambda_3, \lambda_4, \lambda_5$ are the hyperparameters that control the relative contributions of each loss term.

For the structure-contrastive objective, we use a memory-efficient implementation with mini-batch sampling and chunked computations to approximate InfoNCE on large graphs without exceeding GPU memory. Specifically, the similarity function $\text{sim}(\mathbf{h}_v, \mathbf{h}_u)$ operates on the node embedding vectors.

E. Anomaly Inference

During the inference procedure, as detailed in Algorithm 2, GAD-MoRE is deployed on unseen graphs in a zero-shot manner. For each node v , we compute the anomaly score $S(v)$ as the L_2 norm of the residual between the input representation \mathbf{h}_v and its MoE-reconstructed counterpart $\hat{\mathbf{h}}_v$:

$$S(v) = \|\mathbf{h}_v - \hat{\mathbf{h}}_v\|_2. \quad (20)$$

Higher scores indicate greater deviation from curvature-aware normal patterns learned by the Riemannian experts, reflecting reduced reconstruction fidelity and thus stronger evidence of anomalous structure.

V. EXPERIMENTS

In this section, we conduct comprehensive experiments to systematically evaluate our proposed GAD-MoRE framework. The evaluation is designed to answer the following key research questions:

- *RQ1: Overall Performance.* How does GAD-MoRE perform against a wide range of supervised, unsupervised, and state-of-the-art generalist baselines in the challenging zero-shot cross-domain setting?
- *RQ2: Key Component Analysis.* What are the precise contributions of the core innovations in GAD-MoRE, namely the anomaly-aware multi-curvature feature alignment, the mixture of Riemannian experts scorer, and the memory-based dynamic router, to overall model performance?

• *RQ3: Hyperparameter Sensitivity.* How sensitive is GAD-MoRE to its key hyperparameters, such as the embedding dimension and the number of experts, assessing its robustness and practical applicability?

• *RQ4: Comparison with Few-shot Learners.* How does our strictly zero-shot GAD-MoRE model compare against strong generalist competitors that are fine-tuned with a small number of labeled samples from the target graph?

A. Experimental Setup

1) *Datasets:* To evaluate the generalization capability of our model, we conduct experiments on 11 widely used benchmark datasets spanning citation, social, and co-review networks. Following a rigorous protocol, all models are trained on four source graphs (PubMed [15], Flickr [28], [58], Reddit [14], YelpChi [7], [59]) and evaluated on seven unseen target graphs (ACM [60], Amazon [7], [59], BlogCatalog [28], [58], Citeseer [15], Cora [15], Facebook [61], Weibo [14]). Dataset statistics are summarized in Table II.

2) *Baselines:* To ensure a rigorous and fair experimental validation, we benchmark the proposed GAD-MoRE against an extensive collection of competitive methods:

- *Supervised Baselines:* These methods are trained on the source graphs with full label access. We include *GCN* [62], a foundational model that aggregates neighborhood features; *GAT* [63], which uses attention mechanisms for weighted neighbor aggregation; *BWGNN* [64], which applies band-pass filters to amplify high-frequency signals associated with anomalies; and *GHRN* [24], which is designed to handle heterophily in graphs.
- *Unsupervised Baselines:* These methods are trained on the source graphs without any labels. We include *AnomalyDAE* [29], a classic reconstruction-based method using a dual autoencoder for structure and attributes; *CoLA* [21], a contrastive learning framework that learns representations by distinguishing nodes from their corrupted counterparts; and *TAM* [37], which optimizes node embeddings based on a local affinity assumption.
- *Zero-shot Generalist Methods:* These are the current state-of-the-art models designed for zero-shot cross-domain anomaly detection. We include *UNPrompt* [17], which utilizes a unified neighborhood prompting mechanism; *AnomalyGFM* [18], a graph foundation model that learns graph-agnostic prototypes; and the newest *IA-GGAD* [19] framework, which learns invariant representations and structure-insensitive affinities.

3) *Evaluation Metrics:* To evaluate anomaly detection performance comprehensively, we adopt two standard metrics: AUROC and AUPRC, which respectively assess overall discriminative ability and performance on the minority class. To ensure the stability of our findings, we conduct 5 independent runs for every experiment using various random seeds, providing both average results and their corresponding standard deviations.

4) *Implementation Details:* For the detailed hyperparameter settings, the unified feature dimension D after alignment is set to 32. The GNN backbone for structure encoding consists of 4

TABLE III: AUROC results on seven target Graph Anomaly Detection (GAD) datasets. All models are trained exclusively on four source graphs (PubMed, Flickr, Reddit, YelpChi) and evaluated in a zero-shot cross-domain setting. The performance results highlight the optimal outcomes in **bold** and the subsequent best in underline for every dataset. Furthermore, the “Average” column indicates the calculated mean efficacy across the entire suite of benchmarks.

Dataset		Citation			Social			Co-review	
Method		ACM	Citeseer	Cora	BlogCatalog	Facebook	Weibo	Amazon	Average
Supervised	GCN	47.69 \pm 1.48	53.83 \pm 4.01	51.99 \pm 3.20	43.83 \pm 2.39	46.09 \pm 18.88	37.64 \pm 13.84	41.10 \pm 4.24	46.02
	GAT	46.54 \pm 4.71	44.58 \pm 8.25	44.65 \pm 6.20	49.32 \pm 1.70	53.96 \pm 26.14	35.50 \pm 6.91	55.35 \pm 5.69	47.13
	BWGNN	67.43 \pm 2.48	42.58 \pm 2.86	39.75 \pm 3.16	69.91 \pm 4.66	64.84 \pm 4.17	50.08 \pm 0.03	50.01 \pm 0.04	54.94
	GHRN	52.72 \pm 1.01	54.11 \pm 0.88	47.65 \pm 2.03	62.28 \pm 2.42	54.04 \pm 3.81	17.79 \pm 5.00	63.52 \pm 1.92	50.30
Unsupervised	AnomalyDAE	77.60 \pm 1.03	82.00 \pm 2.78	84.01 \pm 1.19	57.53 \pm 0.30	10.87 \pm 0.70	19.77 \pm 1.14	58.38 \pm 0.25	55.74
	CoLA	49.30 \pm 1.00	52.56 \pm 1.36	49.35 \pm 1.52	49.50 \pm 1.27	50.70 \pm 5.49	45.25 \pm 2.39	47.57 \pm 3.02	49.17
	TAM	50.39 \pm 0.08	46.44 \pm 0.15	48.78 \pm 0.17	33.03 \pm 0.28	54.56 \pm 0.36	21.50 \pm 0.30	52.37 \pm 0.12	43.87
Generalist	UNPrompt	73.20 \pm 0.36	59.53 \pm 0.53	63.18 \pm 1.29	70.85 \pm 0.50	60.64 \pm 1.94	66.29 \pm 1.38	72.14 \pm 2.94	66.55
	AnomalyGFM	38.91 \pm 1.21	40.37 \pm 1.37	40.93 \pm 1.09	40.93 \pm 1.22	74.45 \pm 2.36	44.43 \pm 4.89	61.24 \pm 5.21	48.75
	IA-GGAD	78.44 \pm 0.46	91.54 \pm 0.32	85.69 \pm 0.77	73.03 \pm 1.20	69.59 \pm 1.39	87.35 \pm 0.40	53.38 \pm 1.76	77.00
	GAD-MoRE	81.17 \pm 0.05	90.28 \pm 0.13	86.39 \pm 0.20	73.09 \pm 0.06	75.75 \pm 0.95	91.03 \pm 0.11	76.90 \pm 1.80	82.09

TABLE IV: AUPRC results on seven target Graph Anomaly Detection (GAD) datasets. All models are trained exclusively on four source graphs (PubMed, Flickr, Reddit, YelpChi) and evaluated in a zero-shot cross-domain setting. The performance results highlight the optimal outcomes in **bold** and the subsequent best in underline for every dataset. Furthermore, the “Average” column indicates the calculated mean efficacy across the entire suite of benchmarks.

Dataset		Citation			Social			Co-review	
Method		ACM	Citeseer	Cora	BlogCatalog	Facebook	Weibo	Amazon	Average
Supervised	GCN	3.68 \pm 0.16	5.21 \pm 0.89	5.85 \pm 0.55	5.71 \pm 0.38	4.55 \pm 3.06	25.97 \pm 15.84	5.54 \pm 0.51	8.07
	GAT	3.38 \pm 0.45	4.35 \pm 0.82	4.93 \pm 0.75	6.64 \pm 0.71	6.18 \pm 5.83	15.86 \pm 5.83	8.10 \pm 1.24	7.06
	BWGNN	19.48 \pm 2.20	4.02 \pm 0.43	5.30 \pm 0.87	28.37 \pm 4.31	5.71 \pm 1.60	10.47 \pm 0.05	6.79 \pm 0.03	11.45
	GHRN	9.21 \pm 2.94	5.37 \pm 0.14	5.23 \pm 0.19	24.57 \pm 3.60	3.61 \pm 0.68	8.35 \pm 2.44	11.18 \pm 1.10	9.65
Unsupervised	AnomalyDAE	11.67 \pm 0.38	31.37 \pm 1.09	32.65 \pm 1.46	7.17 \pm 0.04	1.32 \pm 0.01	6.10 \pm 0.08	9.26 \pm 1.51	14.22
	CoLA	3.55 \pm 0.12	4.76 \pm 0.21	5.86 \pm 0.34	6.11 \pm 0.36	3.41 \pm 1.38	9.67 \pm 0.50	6.55 \pm 0.44	5.70
	TAM	3.74 \pm 0.01	4.15 \pm 0.02	5.58 \pm 0.08	5.66 \pm 0.17	5.37 \pm 0.51	6.20 \pm 0.02	7.90 \pm 0.05	5.51
Generalist	UNPrompt	24.02 \pm 1.38	9.47 \pm 0.91	10.26 \pm 0.52	35.29 \pm 0.90	3.44 \pm 0.31	28.41 \pm 2.25	<u>12.28</u> \pm 1.63	17.59
	AnomalyGFM	3.10 \pm 0.17	3.69 \pm 0.20	4.36 \pm 0.09	4.85 \pm 0.40	6.00 \pm 0.52	9.05 \pm 1.03	9.18 \pm 1.69	5.75
	IA-GGAD	<u>36.33</u> \pm 0.16	46.96 \pm 1.16	<u>45.03</u> \pm 2.06	36.64 \pm 0.66	<u>8.65</u> \pm 1.74	<u>60.16</u> \pm 0.93	6.90 \pm 0.29	<u>34.38</u>
	GAD-MoRE	37.17 \pm 0.07	<u>40.15</u> \pm 1.31	45.25 \pm 0.88	<u>35.31</u> \pm 0.42	9.00 \pm 1.12	60.26 \pm 0.30	31.55 \pm 4.84	36.96

layers and aggregates information from a 2-hop neighborhood. The final node embeddings are constructed using residual connections to capture deviations from the initial node features. For the MoE scorer, the number of experts K is set to 5, and we use a top- k routing strategy with $k = 2$. The Riemannian experts are initialized with a diverse set of curvatures to cover different Riemannian spaces; specifically, the initial curvatures are set to $[0.0, -0.5, -1.0, 0.5, 1.0]$, allowing experts to specialize in Euclidean, Hyperbolic, and Spherical geometries. The gating mechanism’s softmax temperature is set to 0.7. Then we use the Adam optimizer with a learning rate of 5e-5 and a weight decay of 5e-5, training for 40 epochs on the combined source graphs. The weights for the components in our final loss function (Eq. (19)) are set as $\lambda_1 = 1.0$ ($\mathcal{L}_{\text{embed}}$), $\lambda_2 = 0.5$ ($\mathcal{L}_{\text{feat}}$), $\lambda_3 = 0.1$ ($\mathcal{L}_{\text{struct}}$), $\lambda_4 = 0.1$ (\mathcal{L}_{con}), and $\lambda_5 = 0.01$ ($\mathcal{L}_{\text{gate}}$). For all baselines, we adopt the optimal hyperparameter settings reported in their original papers or tune them on the source graphs. All experiments are conducted

on a single NVIDIA Tesla A100 with 40GB of memory.

B. Overall Performance (RQ1)

The results, as detailed in Table III and Table IV, demonstrate the superiority of our proposed GAD-MoRE framework. Across seven test datasets, GAD-MoRE consistently achieves state-of-the-art performance with an average AUROC of 82.09% and AUPRC of 36.96%, surpassing all baseline categories. Compared to the strongest generalist competitor, IA-GGAD, our model achieves an absolute improvement of 5.09% in average AUROC, validating the effectiveness of our design. Specifically, it establishes a remarkable lead on the structurally complex Weibo dataset, demonstrating the necessity of our specialized Riemannian experts. Notably, GAD-MoRE outperforms even the fully supervised baselines, which have access to anomaly labels on the source graphs. This highlights the limitation of traditional supervised learning in generalizing to new domains and underscores the effectiveness of

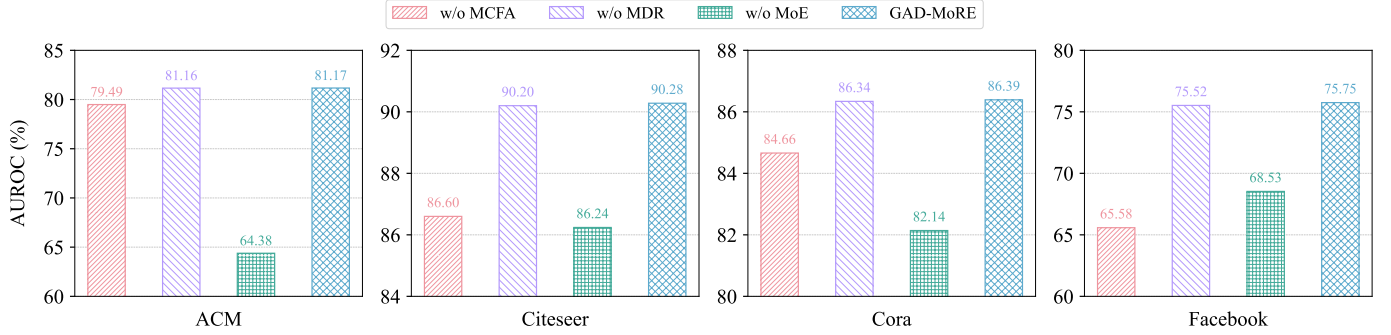


Fig. 3: AUROC performance of GAD-MoRE and its ablation variants on target GAD datasets. All models are trained exclusively on four source graphs (PubMed, Flickr, Reddit, YelpChi) and evaluated in a zero-shot cross-domain setting.

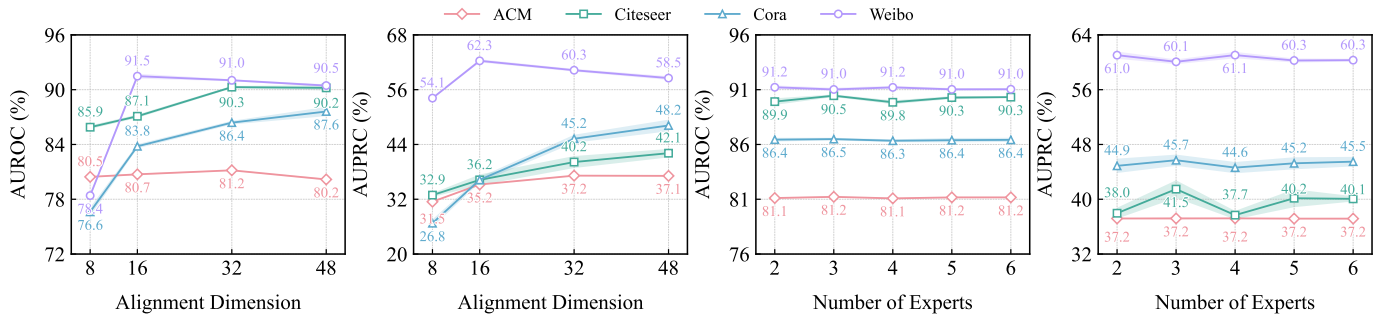


Fig. 4: Hyperparameter sensitivity analysis of GAD-MoRE. The left two subplots show the impact of the unified embedding dimension D on AUROC and AUPRC, while the right two subplots illustrate the sensitivity to the number of experts K .

GAD-MoRE’s unsupervised, geometry-aware approach. When compared to other generalist methods like UNPrompt and AnomalyGFM, GAD-MoRE shows a substantial improvement in both average metrics. This validates our core hypothesis that explicitly modeling the geometric heterogeneity of graphs is crucial for effective domain generalization. The strong AUPRC score is particularly significant, as it confirms that our proposed GAD-MoRE is highly effective at identifying the rare anomalous nodes in an imbalanced setting.

Furthermore, the effectiveness of GAD-MoRE in distinguishing normal from anomalous patterns is visualized in Figure 5, which shows the anomaly score distributions. In both datasets, normal nodes (blue) receive lower scores, while anomalous nodes (red) are assigned higher scores, highlighting GAD-MoRE’s ability to accurately identify anomalies.

C. Key Component Analysis (RQ2)

To answer our second research question and quantify the precise contributions of the central innovations within GAD-MoRE, we conduct a thorough ablation study. We design several variants of our model, each disabling or replacing a key component, and evaluate their AUROC performance against the full model on representative datasets. The components under investigation are: We define the following variants for comparison, with their acronyms matching Figure 3:

- *w/o MCFA*: In this variant, we bypass the MCFA module and use a standard PCA for dimensionality reduction, removing the multi-curvature signals.

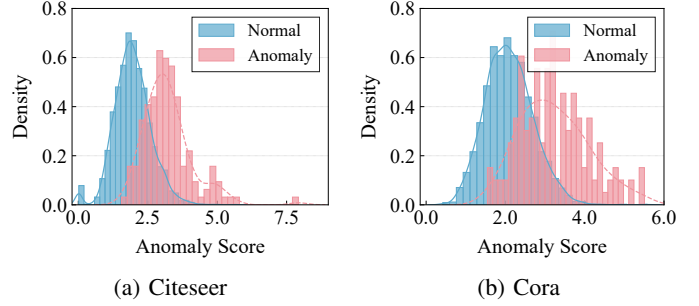


Fig. 5: The anomaly score distributions for Citeseer and Cora show a clear distinction between normal and anomalous nodes. This visual evidence confirms that our approach can effectively detect anomalies in these graph datasets.

- *w/o MoE*: We replace the MoE scorer with an attention-based reconstruction scorer over reference embeddings.
- *w/o MDR*: In this version, we replace our Memory-based Dynamic Router with a simpler linear router.

Figure 3 presents the results of our ablation study. These findings clearly confirm the critical importance of each model component. The most significant performance degradation is observed in the *w/o MoE* variant, with the average AUROC dropping to 75.32%. This provides the strongest empirical evidence for our central hypothesis: a single geometric lens is insufficient for generalizable GAD, and a collection of specialized Riemannian experts is essential for robust performance. By contrast, removing the Multi-curvature Fea-

TABLE V: AUROC performance comparison (in %) of a zero-shot model against few-shot competitors on seven target Graph Anomaly Detection (GAD) datasets. The few-shot methods are fine-tuned with 10 labeled samples (10-shot). The performance results highlight the optimal outcomes in **bold** and the subsequent best in underline for every dataset. Furthermore, the “Average” column indicates the calculated mean efficacy across the entire suite of benchmarks.

Dataset		Citation			Social			Co-review	
Method	ACM	Citeseer	Cora	BlogCatalog	Facebook	Weibo	Amazon	Average	
10-shot	ARC	<u>78.33±1.13</u>	<u>82.31±2.89</u>	<u>82.22±2.34</u>	<u>72.59±1.10</u>	64.94±3.72	<u>88.65±0.82</u>	57.95±6.13	<u>75.28</u>
	AnomalyGFM	41.88±0.73	46.60±0.61	43.56±1.04	38.19±0.34	81.96±3.08	49.68±3.43	<u>66.03±1.91</u>	52.56
0-shot	GAD-MoRE	81.17±0.05	90.28±0.13	86.39±0.20	73.09±0.06	<u>75.75±0.95</u>	<u>91.03±0.11</u>	76.90±1.80	82.09

TABLE VI: AUPRC performance comparison (in %) of a zero-shot model against few-shot competitors on seven target Graph Anomaly Detection (GAD) datasets. The few-shot methods are fine-tuned with 10 labeled samples (10-shot). The performance results highlight the optimal outcomes in **bold** and the subsequent best in underline for every dataset. Furthermore, the “Average” column indicates the calculated mean efficacy across the entire suite of benchmarks.

Dataset		Citation			Social			Co-review	
Method	ACM	Citeseer	Cora	BlogCatalog	Facebook	Weibo	Amazon	Average	
10-shot	ARC	<u>36.53±0.24</u>	<u>30.93±4.24</u>	<u>39.23±4.40</u>	37.77±0.35	4.92±1.85	<u>59.47±2.38</u>	7.98±1.18	<u>30.98</u>
	AnomalyGFM	2.89±0.08	4.13±0.09	4.30±0.10	4.17±0.06	16.53±5.41	9.79±0.99	<u>10.88±1.50</u>	7.53
0-shot	GAD-MoRE	37.17±0.07	40.15±1.31	45.25±0.88	<u>35.31±0.42</u>	9.00±1.12	60.26±0.30	31.55±4.84	36.96

ture Alignment (w/o MCFA) also leads to a substantial performance drop, particularly on the Facebook dataset. This demonstrates that enriching initial node representations with signals from diverse Riemannian spaces provides a more robust foundation, enabling the model to adapt more effectively to unseen graph structures. Lastly, replacing the Memory-based Dynamic Router (w/o MDR) with a simpler linear router results in a slight but consistent performance decrease across most datasets. This highlights the effectiveness of the design of our proposed dynamic routing strategy, as history-aware assignments from the MDR lead to more precise final reconstruction.

D. Hyperparameter Sensitivity (RQ3)

In this section, we investigate the sensitivity of GAD-MoRE to its two most critical hyperparameters: the unified embedding dimension D and the number of experts K . This analysis helps to understand the model’s robustness and guides practical application. Figure 4 illustrates the performance of GAD-MoRE with respect to these two parameters on four representative test datasets, including ACM, Citeseer, Cora, and Weibo.

For the embedding dimension D (left column of Figure 4), we observe that performance for both AUROC and AUPRC generally improves as the dimension increases from 16 to 32. This indicates that a larger dimension allows for more expressive representations to capture complex patterns. However, the performance then stabilizes or slightly decreases for dimension 48, suggesting that overly large dimensions may lead to overfitting on the source datasets without improving generalization. Our chosen value of $D = 32$ offers the best trade-off between performance and model efficiency.

For the number of experts K (right column of Figure 4), performance steadily increases as we add more experts from

$K = 2$ up to $K = 5$. This suggests that a richer set of geometric lenses is beneficial for handling the diverse graph structures encountered in the test sets. Beyond $K = 5$, the performance plateaus, indicating that five experts are sufficient to cover the geometric diversity in our datasets without becoming redundant or introducing unnecessary complexity. This confirms our choice of $K = 5$ as optimal for the MoE scorer. Overall, the results show that GAD-MoRE is robust to variations in these hyperparameters within a reasonable range.

E. Comparison with Few-shot Learners (RQ4)

To further demonstrate the strong performance of our proposed GAD-MoRE on the GAD task, we conduct a comparison against the competitive methods that are fine-tuned using labeled data from the target domain. In particular, we still rigorously evaluate the strictly zero-shot capability of GAD-MoRE in comparing it with few-shot learning approaches, which are allowed access to a limited amount of target-domain labeled data. Specifically, we compare GAD-MoRE with *ARC* [16] and *AnomalyGFM* [18], two representative state-of-the-art generalist GAD frameworks designed for cross-domain transfer. These methods are selected as strong baselines due to their demonstrated effectiveness under few-shot adaptation settings. The baselines are detailed as follows:

- *ARC* [16] utilizes an in-context learning mechanism to adapt to target graphs using limited target labels.
- *AnomalyGFM* [18] is a graph foundation model that aligns node representations with class-agnostic prototypes to achieve generalization.

These two methods are chosen because most traditional GAD models are graph-specific and lack the architectural support for cross-domain fine-tuning. To simulate a competitive few-shot scenario, we fine-tune these baselines on 10 labeled nodes

from each test graph (10-shot) and report performance with our model, which receives no such target-specific advantage.

The quantitative results for AUROC and AUPRC are detailed in Table V and Table VI. Despite operating in a zero-shot setting, GAD-MoRE demonstrates remarkable superiority, achieving an average AUROC of 82.09% and AUPRC of 36.96%. These results substantially surpass the 10-shot fine-tuned ARC (75.28% / 30.98%) and AnomalyGFM (52.56% / 7.53%), proving that GAD-MoRE outperforms competitors on most datasets without access to target domain labels.

This comparison reveals a crucial insight: GAD-MoRE’s architecture is highly effective at learning generalizable, geometry-aware patterns from source domains, enabling it to surpass models that benefit from direct, albeit limited, supervision. This showcases the power of our approach and demonstrates that GAD-MoRE is a more practical and scalable solution for real-world GAD applications where labels for new domains are scarce or entirely unavailable.

VI. CONCLUSION

In this paper, we introduce GAD-MoRE, a novel framework for generalizable graph anomaly detection that addresses the challenge of geometric heterogeneity. Motivated by our empirical finding that no single curvature is universally optimal, we propose a novel MoE architecture, featuring a multi-curvature feature alignment module, a mixture of Riemannian experts scorer, and a memory-based dynamic router. Specifically, the anomaly-aware multi-curvature feature alignment module bridges the gap between geometry-agnostic raw features and manifold representations by projecting inputs into parallel Riemannian spaces. Subsequently, the mixture of Riemannian experts scorer employs specialized Riemannian experts operating in distinct curvature spaces, ensuring that complex anomaly patterns are modeled in suitable geometric environments without distortion. Furthermore, the memory-based dynamic router facilitates adaptive inference using historical reconstruction feedback to align expert selection with the anomaly detection objective. Extensive experiments demonstrate that GAD-MoRE establishes a new state-of-the-art in zero-shot settings and consistently outperforms strong generalist competitors, even those fine-tuned with target domain labels. Promising research directions include extending GAD-MoRE to dynamic graphs, exploring hierarchical MoE architectures, and integrating with graph foundation models.

ACKNOWLEDGMENT

The corresponding author is Qingyun Sun. The authors are supported in part by the National Natural Science Foundation of China through grants No.62225202 and No.62427808, and the Fundamental Research Funds for the Central Universities.

REFERENCES

- [1] Z. Yuan, Q. Sun, H. Zhou, M. Shao, and X. Fu, “A comprehensive survey on gnn-based anomaly detection: taxonomy, methods, and the role of large language models,” *Int. J. Mach. Learn. Cybern.*, pp. 1–26, 2025.
- [2] X. Ma, J. Wu, S. Xue, J. Yang, C. Zhou, Q. Z. Sheng, H. Xiong, and L. Akoglu, “A comprehensive survey on graph anomaly detection with deep learning,” *IEEE TKDE*, vol. 35, no. 12, pp. 12 012–12 038, 2021.
- [3] C. C. Aggarwal, “An introduction to outlier analysis,” in *Outlier analysis*. Springer, 2016, pp. 1–34.
- [4] W. Hilal, S. A. Gadsden, and J. Yawney, “Financial fraud: a review of anomaly detection techniques and recent advances,” *ESWA*, vol. 193, p. 116429, 2022.
- [5] D. Wang, J. Lin, P. Cui, Q. Jia, Z. Wang, Y. Fang, Q. Yu, J. Zhou, S. Yang, and Y. Qi, “A semi-supervised graph attentive network for financial fraud detection,” in *ICDM*. IEEE, 2019, pp. 598–607.
- [6] Y. Yang, Y. Xu, Y. Sun, Y. Dong, F. Wu, and Y. Zhuang, “Mining fraudsters and fraudulent strategies in large-scale mobile social networks,” *IEEE TKDE*, vol. 33, no. 1, pp. 169–179, 2019.
- [7] S. Rayana and L. Akoglu, “Collective opinion spam detection: Bridging review networks and metadata,” in *KDD*, 2015, pp. 985–994.
- [8] S. Kumar, B. Hooi, D. Makhija, M. Kumar, C. Faloutsos, and V. Subrahmanian, “Rev2: Fraudulent user prediction in rating platforms,” in *WSDM*, 2018, pp. 333–341.
- [9] A. B. Nassif, M. A. Talib, Q. Nasir, and F. M. Dakalbab, “Machine learning for anomaly detection: A systematic review,” *IEEE Access*, vol. 9, pp. 78 658–78 700, 2021.
- [10] H. Qiao, H. Tong, B. An, I. King, C. Aggarwal, and G. Pang, “Deep graph anomaly detection: A survey and new perspectives,” *IEEE TKDE*, 2025.
- [11] J. A. Hartigan and M. A. Wong, “Algorithm as 136: A k-means clustering algorithm,” *J. R. Stat. Soc. Ser. C (Appl. Stat.)*, vol. 28, no. 1, pp. 100–108, 1979.
- [12] T. Cover, “Estimation by the nearest neighbor rule,” *IEEE TIT*, vol. 14, no. 1, pp. 50–55, 1968.
- [13] F. T. Liu, K. M. Ting, and Z.-H. Zhou, “Isolation forest,” in *ICDM*. IEEE, 2008, pp. 413–422.
- [14] S. Kumar, X. Zhang, and J. Leskovec, “Predicting dynamic embedding trajectory in temporal interaction networks,” in *KDD*, 2019, pp. 1269–1278.
- [15] P. Sen, G. Namata, M. Bilgic, L. Getoor, B. Galligher, and T. Eliassi-Rad, “Collective classification in network data,” *AI Magazine*, vol. 29, no. 3, pp. 93–93, 2008.
- [16] Y. Liu, S. Li, Y. Zheng, Q. Chen, C. Zhang, and S. Pan, “Arc: A generalist graph anomaly detector with in-context learning,” *NeurIPS*, vol. 37, pp. 50 772–50 804, 2024.
- [17] C. Niu, H. Qiao, C. Chen, L. Chen, and G. Pang, “Zero-shot generalist graph anomaly detection with unified neighborhood prompts,” *ArXiv*, 2024.
- [18] H. Qiao, C. Niu, L. Chen, and G. Pang, “Anomalygfm: Graph foundation model for zero/few-shot anomaly detection,” in *KDD*, 2025, pp. 2326–2337.
- [19] X. Zhang, Z. He, C. Fu, and C. Xie, “Ia-ggad: Zero-shot generalist graph anomaly detection via invariant and affinity learning,” in *NeurIPS*, 2025.
- [20] K. Grover, G. J. Gordon, and C. Faloutsos, “Curvgad: Leveraging curvature for enhanced graph anomaly detection,” in *ICML*, 2025.
- [21] Y. Liu, Z. Li, S. Pan, C. Gong, C. Zhou, and G. Karypis, “Anomaly detection on attributed networks via contrastive self-supervised learning,” *IEEE TNNLS*, vol. 33, no. 6, pp. 2378–2392, 2021.
- [22] T. N. Kipf and M. Welling, “Variational graph auto-encoders,” *ArXiv*, 2016.
- [23] Y. Dou, Z. Liu, L. Sun, Y. Deng, H. Peng, and P. S. Yu, “Enhancing graph neural network-based fraud detectors against camouflaged fraudsters,” in *CIKM*, 2020, pp. 315–324.
- [24] Y. Gao, X. Wang, X. He, Z. Liu, H. Feng, and Y. Zhang, “Addressing heterophily in graph anomaly detection: A perspective of graph spectrum,” in *WWW*, 2023, pp. 1528–1538.
- [25] T. Zhao, X. Zhang, and S. Wang, “Graphsmote: Imbalanced node classification on graphs with graph neural networks,” in *WSDM*, 2021, pp. 833–841.
- [26] L. Wu, J. Xia, Z. Gao, H. Lin, C. Tan, and S. Z. Li, “Graphmixup: Improving class-imbalanced node classification by reinforcement mixup and self-supervised context prediction,” in *ECML-PKDD*, 2022, pp. 519–535.
- [27] K. Liu, H. Zhang, Z. Hu, F. Wang, and P. S. Yu, “Data augmentation for supervised graph outlier detection with latent diffusion models,” *ArXiv*, 2023.
- [28] K. Ding, J. Li, R. Bhanushali, and H. Liu, “Deep anomaly detection on attributed networks,” in *SDM*. SIAM, 2019, pp. 594–602.
- [29] H. Fan, F. Zhang, and Z. Li, “Anomalydae: Dual autoencoder for anomaly detection on attributed networks,” in *ICASSP*. IEEE, 2020, pp. 5685–5689.
- [30] X. Yuan, N. Zhou, S. Yu, H. Huang, Z. Chen, and F. Xia, “Higher-order structure based anomaly detection on attributed networks,” in *IEEE BigData*. IEEE, 2021, pp. 2691–2700.

[31] P. Veličković, W. Fedus, W. L. Hamilton, P. Liò, Y. Bengio, and R. D. Hjelm, “Deep graph infomax,” *ArXiv*, 2018.

[32] F.-Y. Sun, J. Hoffmann, V. Verma, and J. Tang, “Infograph: Unsupervised and semi-supervised graph-level representation learning via mutual information maximization,” *ArXiv*, 2019.

[33] F. Lin, X. Luo, J. Wu, J. Yang, S. Xue, Z. Wang, and H. Gong, “Discriminative graph-level anomaly detection via dual-students-teacher model,” in *ADMA*. Springer, 2023, pp. 261–276.

[34] Z. Chen, B. Liu, M. Wang, P. Dai, J. Lv, and L. Bo, “Generative adversarial attributed network anomaly detection,” in *CIKM*, 2020, pp. 1989–1992.

[35] K. Ding, J. Li, N. Agarwal, and H. Liu, “Inductive anomaly detection on attributed networks,” in *IJCAI*, 2021, pp. 1288–1294.

[36] K. Ding, Q. Zhou, H. Tong, and H. Liu, “Few-shot network anomaly detection via cross-network meta-learning,” in *WWW*, 2021, pp. 2448–2456.

[37] S. Tian, J. Dong, J. Li, W. Zhao, X. Xu, B. Wang, B. Song, C. Meng, T. Zhang, and L. Chen, “Sad: semi-supervised anomaly detection on dynamic graphs,” in *IJCAI*, 2023, pp. 2306–2314.

[38] R. A. Jacobs, M. I. Jordan, S. J. Nowlan, and G. E. Hinton, “Adaptive mixtures of local experts,” *Neural Comput.*, vol. 3, no. 1, pp. 79–87, 1991.

[39] N. Shazeer, A. Mirhoseini, K. Maziarz, A. Davis, Q. Le, G. Hinton, and J. Dean, “Outrageously large neural networks: The sparsely-gated mixture-of-experts layer,” in *ICLR*, 2017.

[40] Z. Mi, P. Yin, X. Xiao, and D. Xu, “Learning heterogeneous mixture of scene experts for large-scale neural radiance fields,” *IEEE TPAMI*, 2025.

[41] W. Fedus, B. Zoph, and N. Shazeer, “Switch transformers: Scaling to trillion parameter models with simple and efficient sparsity,” *JMLR*, vol. 23, no. 120, pp. 1–39, 2022.

[42] C. Riquelme, J. Puigcerver, B. Mustafa, M. Neumann, R. Jenatton, A. Susano Pinto, D. Keysers, and N. Houlsby, “Scaling vision with sparse mixture of experts,” *NeurIPS*, vol. 34, pp. 8583–8595, 2021.

[43] L. Liu, P. Wang, G. Wu, J. Jiang, and H. Yang, “Towards optimal mixture of experts system for 3d object detection: A game of accuracy, efficiency and adaptivity,” *IEEE TPAMI*, 2025.

[44] Z. Guo, Q. Sun, H. Yuan, X. Fu, M. Zhou, Y. Gao, and J. Li, “Graphmore: Mitigating topological heterogeneity via mixture of riemannian experts,” in *AAAI*, vol. 39, no. 11, 2025, pp. 11754–11762.

[45] H. Zeng, H. Lyu, D. Hu, Y. Xia, and J. Luo, “Mixture of weak & strong experts on graphs,” *ArXiv*, 2023.

[46] H. Wang, Z. Jiang, Y. You, Y. Han, G. Liu, J. Srinivasa, R. Kompella, Z. Wang *et al.*, “Graph mixture of experts: Learning on large-scale graphs with explicit diversity modeling,” *NeurIPS*, vol. 36, pp. 50825–50837, 2023.

[47] F. Hu, L. Wang, S. Wu, L. Wang, and T. Tan, “Graph classification by mixture of diverse experts,” *ArXiv*, 2021.

[48] J. Cai, Y. Zhang, P. Wang, and S.-K. Ng, “Moegad: A mixture-of-experts framework with pseudo-anomaly generation for graph-level anomaly detection,” *IEEE TPAMI*, 2025.

[49] I. Chami, Z. Ying, C. Ré, and J. Leskovec, “Hyperbolic graph convolutional neural networks,” *NeurIPS*, vol. 32, 2019.

[50] X. Fu, J. Li, J. Wu, Q. Sun, C. Ji, S. Wang, J. Tan, H. Peng, and P. S. Yu, “Ace-hggn: Adaptive curvature exploration hyperbolic graph neural network,” in *ICDM*. IEEE, 2021, pp. 111–120.

[51] J. Li, X. Fu, Q. Sun, C. Ji, J. Tan, J. Wu, and H. Peng, “Curvature graph generative adversarial networks,” in *WWW*, 2022, pp. 1528–1537.

[52] R. C. Wilson, E. R. Hancock, E. Pekalska, and R. P. Duin, “Spherical and hyperbolic embeddings of data,” *IEEE TPAMI*, vol. 36, no. 11, pp. 2255–2269, 2014.

[53] M. Nickel and D. Kiela, “Poincaré embeddings for learning hierarchical representations,” *NeurIPS*, vol. 30, 2017.

[54] Q. Liu, M. Nickel, and D. Kiela, “Hyperbolic graph neural networks,” *NeurIPS*, vol. 32, 2019.

[55] Y. Zhang, X. Wang, C. Shi, X. Jiang, and Y. Ye, “Hyperbolic graph attention network,” *IEEE TBD*, vol. 8, no. 6, pp. 1690–1701, 2021.

[56] K. Pearson, “Lii. on lines and planes of closest fit to systems of points in space,” *The London, Edinburgh, and Dublin philosophical magazine and journal of science*, vol. 2, no. 11, pp. 559–572, 1901.

[57] H. Hotelling, “Analysis of a complex of statistical variables into principal components,” *J. Educ. Psychol.*, vol. 24, no. 6, p. 417, 1933.

[58] L. Tang and H. Liu, “Relational learning via latent social dimensions,” in *KDD*, 2009, pp. 817–826.

[59] J. J. McAuley and J. Leskovec, “From amateurs to connoisseurs: modeling the evolution of user expertise through online reviews,” in *WWW*, 2013, pp. 897–908.

[60] J. Tang, J. Zhang, L. Yao, J. Li, L. Zhang, and Z. Su, “Arnetminer: extraction and mining of academic social networks,” in *KDD*, 2008, pp. 990–998.

[61] Z. Xu, X. Huang, Y. Zhao, Y. Dong, and J. Li, “Contrastive attributed network anomaly detection with data augmentation,” in *PAKDD*. Springer, 2022, pp. 444–457.

[62] T. Kipf, “Semi-supervised classification with graph convolutional networks,” *Arxiv*, 2016.

[63] P. Veličković, G. Cucurull, A. Casanova, A. Romero, P. Lio, and Y. Bengio, “Graph attention networks,” *ArXiv*, 2017.

[64] J. Tang, J. Li, Z. Gao, and J. Li, “Rethinking graph neural networks for anomaly detection,” in *ICML*, 2022, pp. 21076–21089.

Xinyu Zhao is currently a master’s candidate at the School of Computer Science and Engineering, Beihang University. His research interests include graph anomaly detection and graph foundation models.

Qingyun Sun is currently an Associate Professor at the School of Computer Science and Engineering, Beihang University. Her research interests include machine learning and graph mining. She has published several papers on IEEE TPAMI, IEEE TKDE, Web Conference, AAAI, ICDM, CIKM, *etc.*

Jiayi Luo is currently a Ph.D. candidate at the School of Computer Science and Engineering, Beihang University. His research interests include robust graph learning and graph foundation models.

Xingcheng Fu is currently an associate professor at the Key Lab of Education Blockchain and Intelligent Technology at Guangxi Normal University. His research interests include graph representation learning, complex networks, and social network analysis. He has published several papers on IEEE TKDE, Web Conference, AAAI, ICDM, CIKM, *etc.*

Jianxin Li is currently a Professor with the School of Computer Science and Engineering, Beihang University. His current research interests include social networks, machine learning, big data, and trustworthy computing. Dr. Li has published research papers in top-tier journals and conferences, including the IEEE TKDE, TDSC, JAIR, ACM TOIS, TKDD, KDD, AAAI, and WWW.